Impact of powder reusability on batch repeatability of Ti6Al4V ELI for PBF-LB industrial production

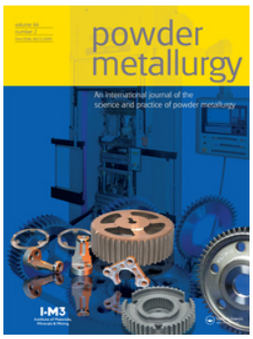

Powder Metallurgy

ISSN: (Print) (Online) Journal homepage: https://www.tandfonline.com/loi/ypom20

Impact of powder reusability on batch repeatability of Ti6Al4V ELI for PBF-LB industrial production

Laura Cordova, Cindy Sithole, Eric Macía Rodríguez, Ian Gibson & Mónica Campos

To cite this article: Laura Cordova, Cindy Sithole, Eric Macía Rodríguez, Ian Gibson & Mónica Campos (2023) Impact of powder reusability on batch repeatability of Ti6Al4V ELI for PBF-LB industrial production, Powder Metallurgy, 66:2, 129-138, DOI: 10.1080/00325899.2022.2133357

To link to this article: https://doi.org/10.1080/00325899.2022.2133357

Published online: 18 Oct 2022.

POWDER METALLURGY
2023, VOL. 66, NO. 2, 129–138
https://doi.org/10.1080/00325899.2022.2133357

I·M3 Institute of Materials, Minerals & Mining
Taylor & Francis Taylor & Francis Group

RESEARCH ARTICLE

Impact of powder reusability on batch repeatability of Ti6Al4V ELI for PBF-LB industrial production

Laura Cordova [a,b,c], Cindy Sithole[d], Eric Macía Rodríguez[e], Ian Gibson [b,d] and Mónica Campos [e]

[a]Department of Mechanics of Solids, Surfaces & Systems (MS3), University of Twente, Enschede, The Netherlands; [b]Design, Production & Management, Fraunhofer Innovation Platform for Advanced Manufacturing at the University of Twente, Enschede, The Netherlands; [c]Department of Industrial and Materials Science, Chalmers University of Technology, Gothenburg, Sweden; [d]Department of Design, Production and Management, University of Twente, Enschede, The Nertherlands; [e]Department of Materials Science and Engineering, University Carlos III of Madrid, Leganés, Spain

ABSTRACT

In powder bed fusion laser beam (PBF-LB), powder reusability remains key to keeping cost-effectivity as well as sustainability. In this study, highly sensitive Ti6Al4V ELI powder typically used for medical and aerospace applications is studied. Powder properties of new and reused powders after 10 build cycles subjected to variations such as morphology, particle size distribution (PSD), chemical composition and flowability were analysed. The flow rate using Carney flowmeter increased from 6.8 s to 12 s. Oxygen content slightly increased from 0.11% to 0.12%. The dimensional deviations are measured in six builds of eight samples spread through the build plate. The density of the cubes does not show relevant differences in density (from 99.6% to 99.9%), only the last batch exhibits slightly lower density than the previous builds. Studied properties for the powder and builds are maintained throughout the experiment, demonstrating repeatability of industrial production of metal parts.

ARTICLE HISTORY
Received 25 May 2022
Revised 14 September 2022
Accepted 1 October 2022

KEYWORDS
Powder reusability; powder bed fusion laser beam (PBF-LB); Ti6Al4V ELI; grade 23; repeatability; batch production; industrial AM

1. Introduction

During the powder bed fusion laser beam (PBF-LB) process, a layer of metal powder is initially deposited to be then melted by a laser beam. Since only a small portion of the powder is transformed into a solid 3D part based on an STL file, the rest of the powder is reused in consecutive builds with a sieving step in between each time [1]. This, ideally, would result in a zero-(powder) waste production. However, in heavily regulated industries, like aerospace where process and part certification play a key role, the uncertainties of reusing the powder prevent unlimited powder usage.

When reusing all the powder, the material efficiency can be up to 95% [2]. Therefore, it is of paramount importance that the powder does not age both during storage and reuse. During reuse, laser hours are one of the key factors that can influence powder properties. For example, using four lasers for a lengthy job in which the powder will be in contact with a portion of oxygen and other contaminants under high-temperature conditions can lead to a high risk of pickup of contaminants. The spattering behaviour of the alloying elements can also influence the efficiency of reuse as discussed by Gesper et al. [3,4]. Consequently, condensates are generated, and these can show differences in morphology and particle size distribution (PSD). Not all alloys are equally impacted by the same amount of reuse as discussed by the authors in a previous study [5]. Certain alloying elements have a higher affinity for oxygen and tend to oxidise faster as studied by Mellin et.al. [6]. For every new alloy, besides processability and quality tests, the reusability must be investigated following a methodology as proposed by Sutton et al. [7].

In general, powder properties, such as chemical composition, morphology, PSD, flowability and apparent density are impacted by reuse after a few cycles as determined in previous work by Cordova et al. [8] for Scalmalloy. The variations in PSD towards coarser size and less fraction of particles fines impacted the level of porosity in the final builds.

Seyda et al. [9] investigated the effect of reusing Ti6Al4V during 12 cycles in a LPBF machine in which the average particle size increased from 37.4 to 51.2 µm and the number of fine particles was reduced, this had a positive effect on the flowability and apparent density that increased by 9%. Additionally, after 21 cycles, Ti6Al4V showed significant changes in the morphology and PSD as demonstrated by Tang et al. [10], these variations did not have a large influence on the mechanical properties which showed homogenous results irrespective of the location on the powder bed. Due to coarsening, the reused powder

CONTACT Laura Cordova laura.cordova@chalmers.se Department of Mechanics of Solids, Surfaces & Systems (MS3), University of Twente, Drienerlolaan 5, Enschede 7522 NB, The Netherlands

Table 1. Chemical composition (wt.%) Ti6-Al4-V grade 23 used in this study.

Element	Ti	Al	V	Fe	C	N	H	Other, each	Other, total
Content (%)	88.09–91	5.5–6.5	3.5–4.5	≤0.25	≤0.080	≤0.030	≤0.0125	≤0.10	≤0.40

tends to show improved flowability. In general, Ti6Al4V shows increments in oxide content, in the case of ELI (grade 23) there is a limit established at 0.13% for biomedical applications by ASTM F136 - 13(2021)e1 standardisation. In a study of the oxygen content of the powder and built part throughout five build cycles, O'Leary et al. [11] found a larger oxygen content in the Ti6Al4V parts of around 0.2% than in the powder, circa 0.13%. There is evidence reuse impacts porosity level, tensile strength and elongation as determined by Quintana et al. [12] for Ti6Al4V ELI. In their study, the authors found an increase of oxygen content up to 0.13% after 31 builds, fewer fines in the particle size which led to improved flowability and a strengthening effect lead by the higher oxygen content. Since oxygen is an α-stabiliser, an increase in the oxygen content upon reuse can increase the material strength and hardness at the cost of ductility and fracture toughness [13]. Similar findings were reported by Denti et al. [14] and Harkin et al. [15] on grade 23 for which an interstitial solid solution strengthening mechanism was reported. Alamos et al. [16] investigated powder reuse for eight cycles using different energy densities in 30 and 60 µm builds. No differences were observed in static mechanical behaviour upon reuse. The oxygen content slightly increased towards the eight cycles.

In this study, the link between powder reusability and batch repeatability is established by means of powder characterisation and built parts measurements. The state-of-the-art has demonstrated that oxygen pick up is a common issue when reusing Ti6Al4V grade 23 in addition to variations in morphology and particle size impacting flowability and apparent density. However, batch repeatability assessment throughout consecutive builds has not been linked to powder reusability yet. In total six builds were studied in which the dimensional deviations, as well as density and microstructure, are analysed. This is studied to demonstrate the challenges in batch repeatability from build to build and within the same build using an industrial system equipped with two laser sources, a close loop powder handling system and a large build plate (420 × 420 × 400 [mm]).

2. Materials and methods

In this study, powder reusability and batch repeatability will be studied. The powder was supplied by Additive Industries to ASTM F3001 standard specification with a particle range between 15 and 45 µm. The elemental chemical composition of the Ti6Al4V ELI – grade 23 powder is shown in Table 1. Ti6Al4V ELI, short for 'Extra Low Interstitials', contains reduced levels of oxygen, nitrogen, carbon and iron. These lower interstitials provide improved ductility and better fracture toughness for Ti6Al4V. This grade with the highest purity is often used for medical applications.

For this study, the MetalFAB1 machine by Additive Industries, The Netherlands has been used. On the one hand, the virgin powder was collected and analysed together with reused powder for a period of time that comprised about ten complete build cycles. During the laser powder bed fusion (LPBF), process metal powder is loaded into the machine for multiple builds. In the MetalFAB1 machine equipped with two Yb fibre lasers of power 500 W, after every build cycle, the powder on the build plate is removed by an automatic extraction system. This is followed by sieving and storage in a protective atmosphere by the transport gas, in this case, Argon with quality 99.99999%. When the building process is taking place the process gas is filtered to ensure the powder is under optimal conditions for maximum quality. Particle and microstructural characterisation of two batches of Ti6Al4V ELI powders have been the scope of this work. The two batches are tested at two different processing steps before and after usage in the PBF-LB process. Therefore, the selected nomenclature is virgin (1) and reused (2) powder.

On the other hand, density cubes (Figure 1(c)) were built on the MetalFAB1 consecutively in six different build jobs by using the standard process parameters optimised for this material by Additive Industries with two laser beams as shown in Figure 1(a), laser 3 and laser 4. The cube dimensions represented in a STL file are 15 mm per side. The aim of placing the density cubes spread on the build plate was to measure the variation of properties on different locations (i.e. close to the inlet/outlet gas nozzles and from left to right following the recoater trajectory, as shown in Table 2 and Figure 1(a,b)). The first five build jobs were carried out before an update to the second gas nozzle flow; which was aimed to improve the gas flow distribution in the build chamber in particular during bulky and lengthy build jobs in which higher gas flow rate is required to effectively remove condensates and contaminants generated during the PBF-LB process.

Properties such as morphology, chemical composition (on elemental and interstitial levels), flowability and packing density were tested. Morphology study and composition analysis of powder batches pass by scanning electron microscopy (SEM) observation. Virgin powder (1) characteristics' using a voltage

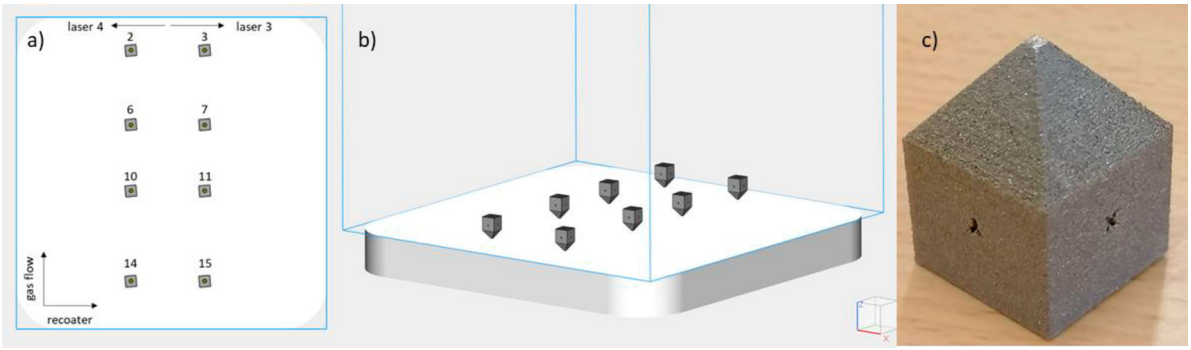

Figure 1. Location of the samples on the build plate from Z direction (a) from XY direction (b), sample geometry placed upside down (c).

of 10 kV, current of 0.20 nA for the particle morphology and 0.40 nA for the cross-sections with a working distance of 10 mm. The powder was embedded using a conductive resin followed by a conventional metallographic preparation to study the powder cross-sectional area with the FEG SEM (FEI). Semiquantitative composition measurement was done by an EDS detector (Energy-dispersive X-ray spectroscopy). C and S content was measured by LECO CS-200; meanwhile, the O and N content was determined by the equipment LECO TC-500. The PSD was measured using the laser diffraction technique by the MASTERSIZER 2000 (Malvern Panalytical) using water as a dispersant agent.

The apparent density and the flow rate were determined by the use of a Hall funnel following the ASTM B964 and ASTM B212 standard specifications respectively. The tap density was done with a Quantachrome Autotap AT-6 following the ASTM B527 standard specification. With the data obtained from the measurements, the Hausner ratio is calculated by the relation between the tap and the apparent density as described in Equation (1).

$$\mathrm{HR} = \frac{\rho_{\mathrm{tap}}}{\rho_{\mathrm{apparent}}} \tag{1}$$

The Carr's compressibility Index (CI) establishes a relationship between the starting volume (V_{starting}) of powder and the one measured after the tap test (V_{final}), as shown in Equation (2).

$$\mathrm{CI} = \frac{V_{\mathrm{starting}} - V_{\mathrm{final}}}{V_{\mathrm{starting}}} \tag{2}$$

Table 2. Sample number and location on the build plate.

Sample No.	*x*-Coordinate	*y*-Coordinate
2	−55	165.15
3	45	165.15
6	−55	65.15
7	45	65.15
10	−55	−24.06
11	45	−24.06
14	−55	−145.63
15	45	−145.63

Finally, the repose angle is determined by Equation (3).

$$\text{Repose angle} = \tan^{-1}\left(\frac{2H}{D}\right) \tag{3}$$

where H is the height of the powder after passing through the Hall funnel and D is the diameter of the cup in which the powder is collected.

The cubes were tested on dimensional deviations using a digital calliper with an uncertainty of 0.005 mm and density following Archimedes' principle to ASTM B962 standard specification. The density measurements were performed using Archimedes' test principle and the ASTM standard for density measurement was followed. The tests were conducted using water for measurements in fluid. A tiny droplet of soap, as deflocculant, was added to the water to reduce the surface tension of the samples. The test was conducted three times.

3. Results and discussion

3.1. Powder properties

The morphological features and shape of the powder particles were studied by SEM as shown in Figure 2. Different magnifications were used to observe the details of both particle surface and cross-sections. High magnification images of virgin and reused particles do not show large differences between them, in fact, after 10 build cycles neither shape nor size is affected, only satellites seem to be less frequent in reused powder. Figure 2(c,d) offers a close perspective of a particle, in 2(c) the clear atomisation dendrites can be observed, unlike 2(d) in which the reuse powder particle shows a more oxidised surface typically found in Ti6Al4V as discussed by Pauzon et al. [17]. Cross-sectional images show the typical microstructure of pristine atomised Ti6Al4V powder, with minimal internal porosity.

The images in Figure 3 are aimed to provide a more precise detail of the powders. It seems that the reused powder shares similar irregularities than the virgin

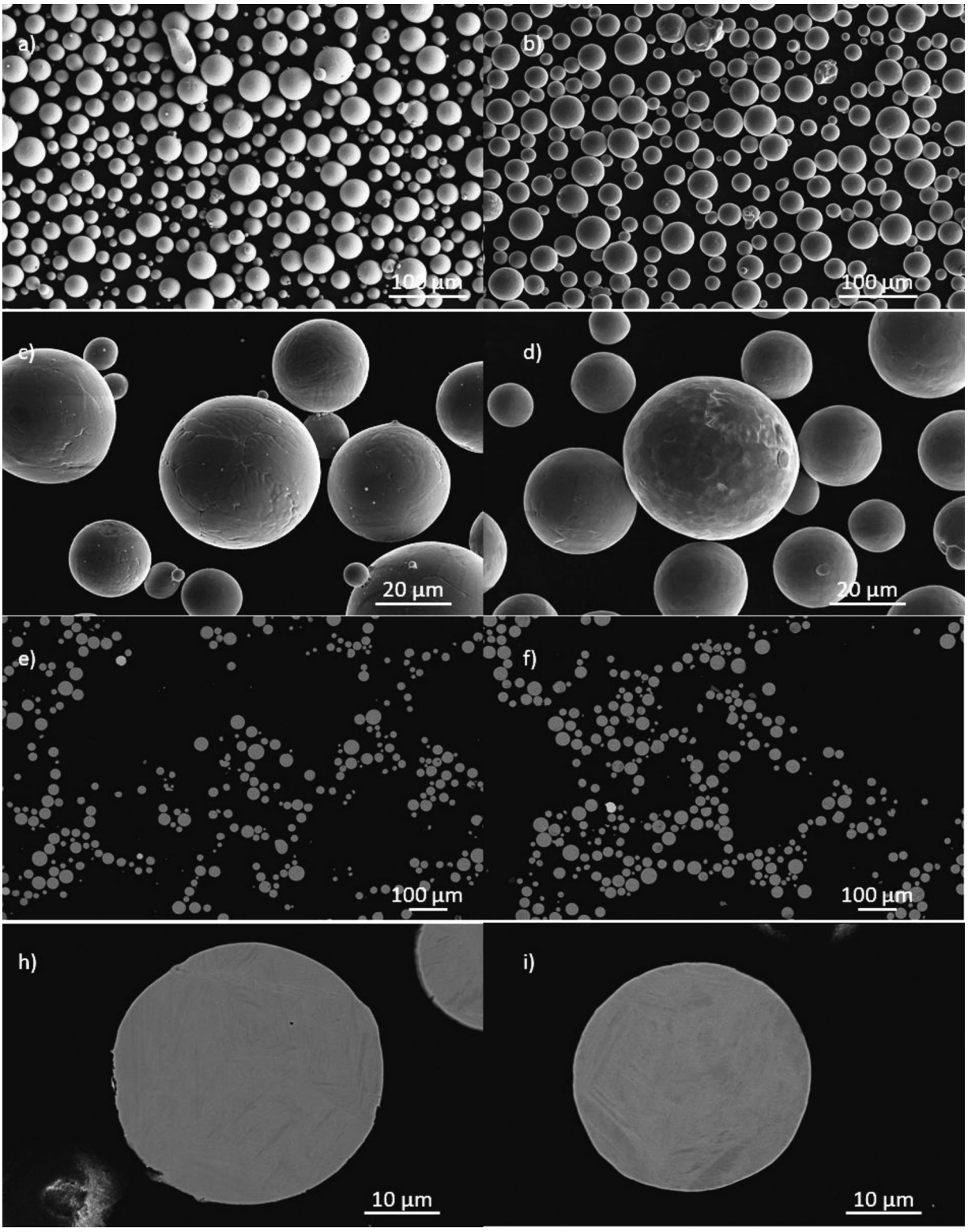

Figure 2. Virgin (a, c, e, h) and reused (b, d, f, i) powder images. Deposited virgin powder (a, c), deposited reused powder (e, h), cross-section virgin powder (e, F) and cross-section reused powder (h, i). The magnifications used are 200×, 1000×, 100× and 2000×, in order of appearance.

powder, where satellites and features due to second collisions during atomisation can be seen, but it is true that very few particles seem to be affected. In general, fewer fines are spotted in reused powder in comparison with virgin powder. PSD measurements are rarely able to detect this difference by laser diffraction, so measurements of fine particle fractions are limited.

Figure 4 shows a *moderate* increase in the size of the powder during PBF-LB processing. This has been discussed before for Inconel 718 powder reused during 14 cycles by Ardila et al. [2], the reason for the increase in particle size was given to particle aggregations. However, Table 3 shows more detail on the distribution since for lower particle size fractions the

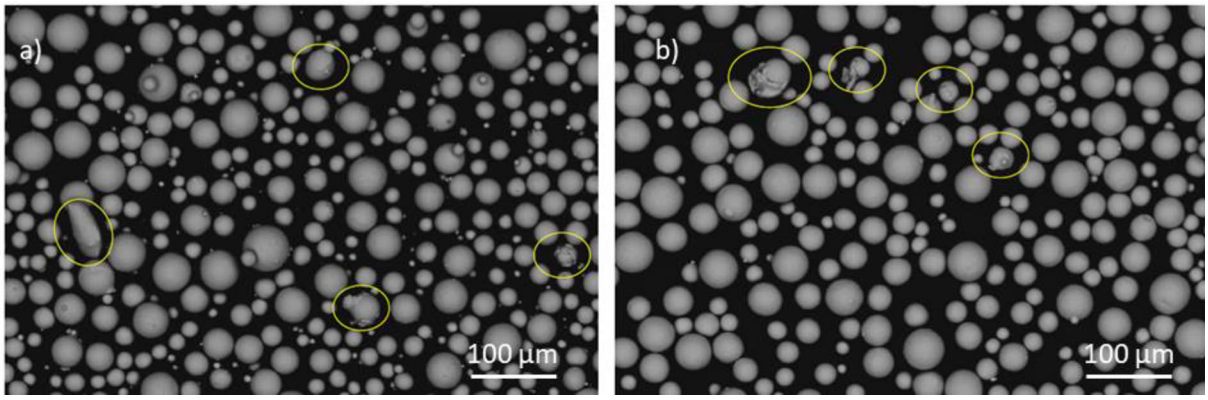

Figure 3. Virgin (a) and reused (b) powder, observation of irregular particles marked with yellow circles.

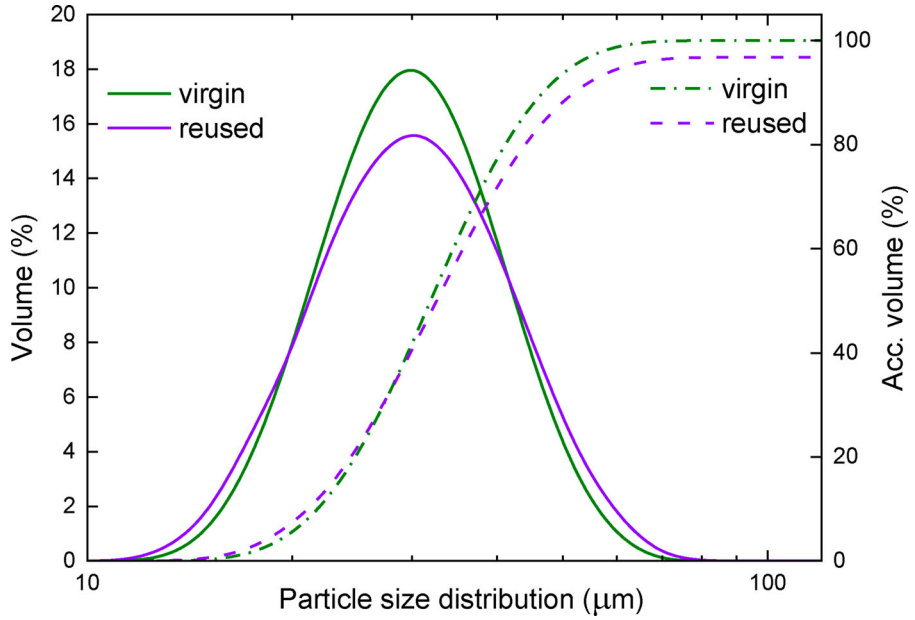

Figure 4. Particle size distribution of virgin and reused powders. Volume of particles per size (left axis), accumulated volume of particles per size (right axis).

value has slightly decreased from reuse, this could be attributed to the presence of condensates of lower size than the original PSD. Hence, due to fine particles are lighter, they get carried away into the transport gas system getting stuck to pipe/walls. In this case, the variation is also very moderate; it is necessary to study if this has an influence on its packing ability or flowability.

The results of the bulk chemical content of interstitial elements (oxygen, nitrogen, carbon and sulphur) are shown in Table 4. There are no remarkable differences between the two batches, only oxygen content shows a slight increase beyond the standard deviation. This is due to oxygen pickup despite the protection purging the chamber inert gas, some of this contamination can be picked up by condensates and oxidised particles as part of the melting process as discussed by Pauzon et al. [18]. The essential difference between Ti6Al4V ELI (grade 23) and Ti6Al4V (grade 5) is the lower oxygen content of the first one, with a maximum value of 0.13% according to ASTM F3001.

Table 3. Parameters of the particle size distribution.

Sample	d10 [µm]	d50 [µm]	d90 [µm]
Virgin powder (1)	18.33	28.46	46.02
Reused powder (2)	15.96	30.39	49.32

The results of a semiquantitative composition measurement done by an EDS detector are displayed in Table 5. There are no differences between the two batches and the values are within the nominal composition (Table 1). Hence, the PBF-LB processing has not affected the elemental composition. The similarity on result values demonstrated that there is no variation in composition as a consequence of the reuse of the powder.

Table 6 shows the results of the measurements described by the above equations. In order to evaluate the influence of the values of the angle of repose, the

Table 4. Interstitial elements content for virgin powder (1) and reused powder (2).

Powder Batch	O [wt%]	N [wt%]	C [wt%]	S [wt%]
Virgin powder (1)	0.110 ± 0.004	0.0020 ± 0.0002	0.017 ± 0.001	0.0040 ± 0.0003
Reused powder (2)	0.120 ± 0.001	0.0020 ± 0.0002	0.019 ± 0.001	0.0049 ± 0.0007

Table 5. Batch composition analysed by EDS.

Powder batch	Ti [wt%]	Al [wt%]	V [wt%]
Virgin powder (1)	90.02 ± 1.57	6.31 ± 7.66	3.66 ± 7.90
Reused powder (2)	89.79 ± 1.57	6.16 ± 7.66	4.05 ± 6.93
Nominal composition range	88.09–91	5.5–6.5	3.5–4.5

Nominal alloy: Ti6Al4V-23 (chemical composition in Table 1).

Table 6. Flowability and tapping density measurement results.

	Virgin powder (1)	Reused powder (2)
Flow rate Hall [s]	37 ± 3	NA
Flow rate Carney [s]	6.8 ± 0.4	12 ± 0.5
App density [g cm^{-3}]	2.49 ± 0.01	2.49 ± 0.01
Tap density [g·cm^{-3}]	2.86 ± 0.05	2.88 ± 0.02
Carr index [%]	11 ± 1	12.0 ± 0.7
Hausner ratio[–]	1.15 ± 0.02	1.15 ± 0.01
Repose angle [°]	28 ± 1	30 ± 2

Carr index and the Hausner ratio, an accepted scale has been considered [19]. Both batches show values between Excellent and Good in the consulted scale. Given the flow rate using Carney funnel, with a larger aperture than Hall, reused powder shows a better rheological behaviour. This could be explained by the slightly larger PSD. However, the reused powder did not flow when tested by the Hall flowmeter, which is not uncommon for powder used in PBF-LB [20,21].

3.2. As-built part repeatability

The process repeatability is studied from two perspectives: (i) based on the location of the density cubes on the build plate and (ii) during consecutive build cycles. The cubes were spread on the build plate as shown in Figure 1. The numbering shown in the image will be followed by the test. Note that two lasers were used, on the left and right side on the plate divided by the middle *y*-axis. In the figure, also recoater and gas flow direction (outlet to inlet) are represented. The numeration of samples increases towards the gas inlet which is also located at the machine glass window. Dimensional deviation from the nominal size based on the STL file was measured following both the X and Y directions shown in Figure 1(b), in which X is parallel to the movement on the recoater and Y is parallel to the gas flow. The results of these measurements are shown in Figure 5. Three readings were taken on each side of the reference and were separated as bottom, middle and top. The average of the results was plotted, and the standard deviation was calculated on the three measurements based on two decimals of accuracy.

For the first three batches, the measured dimensions follow the similar trend in both X and Y directions, similarly to batches five and six. Batch 4 shows measures with similar values in all locations, always below the nominal values, with deviations in average between −1.5% and −2% as shown in Table 7. In general, the deviations from the first three batches show more varying deviations than the latter three. Despite manufacturing with two different laser beams, it seems that differences in deviations are, in general, mainly location based since samples 2 and 3, 6 and 7, 10 and 11, and 14 and 15 exhibit similar dimensions independently of the batch number. In fact, similarities on samples located at the same point of *y*-coordinates indicate a dependence of the dimensional accuracy on the gas flow. Now, for the first three batches' samples 14 and 15 show values similar or over the nominal dimensions respectively, unlike the rest of the cubes in which their values show negative deviations (Table 7). The heating and cooling profile of samples closer to the gas inlet versus gas outlet can show differences due to the cooling effect of the gas.

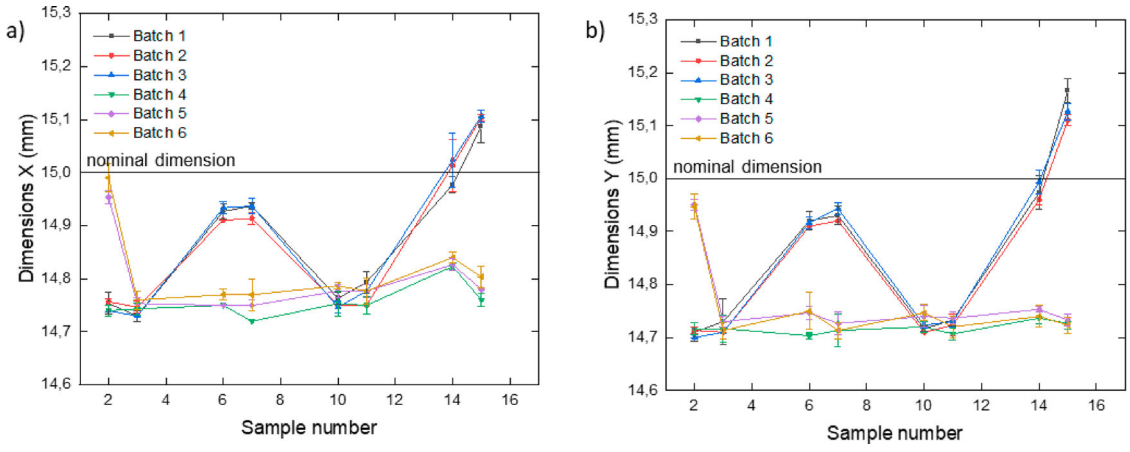

Figure 5. Measured dimensions in X (a) and Y (b) direction, parallel to the recoater and gas flow, respectively.

Table 7. Dimensional deviations in % from nominal measures in *x* and *y* directions.

Sample No.	Batch 1		Batch 2		Batch 3		Batch 4		Batch 5		Batch 6	
	x	*Y*	*X*	*y*	*x*	*y*	*X*	*y*	*x*	*y*	*x*	*y*
2	−1.64%[a]	−1.93%[a]	−1.62%[a]	−1.91%[a]	−1.73%[a]	−2.00%[a]	−1.73%[a]	−1.89%[a]	−0.31%[b]	−0.33%[b]	−0.07%[b]	−0.36%[b]
3	−1.80%[a]	−1.80%[a]	−1.69%[a]	−1.93%[a]	−1.80%[a]	−1.93%[a]	−1.71%[a]	−1.89%[a]	−1.64%[a]	−1.80%[a]	−1.60%[a]	−1.91%[a]
6	−0.49%[b]	−0.53%[b]	−0.60%[b]	−0.60%[b]	−0.44%[b]	−0.56%[b]	−1.67%[a]	−1.98%[a]	−1.67%[a]	−1.69%[a]	−1.53%[a]	−1.67%[a]
7	−0.42%[b]	−0.47%[b]	−0.58%[b]	−0.53%[b]	−0.42%[b]	−0.38%[b]	−1.87%[a]	−1.91%[a]	−1.67%[a]	−1.82%[a]	−1.53%[a]	−1.91%[a]
10	−1.58%[a]	−1.89%[a]	−1.67%[a]	−1.93%[a]	−1.69%[a]	−1.84%[a]	−1.64%[a]	−1.87%[a]	−1.49%[a]	−1.73%[a]	−1.42%[a]	−1.69%[a]
11	−1.38%[a]	−1.78%[a]	−1.67%[a]	−1.84%[a]	−1.49%[a]	−1.80%[a]	−1.67%[a]	−1.96%[a]	−1.49%[a]	−1.76%[a]	−1.49%[a]	−1.87%[a]
14	−0.16%[b]	−0.18%[b]	0.09%[c]	−0.27%[b]	0.16%[c]	−0.04%[b]	−1.18%[a]	−1.76%[a]	−1.16%[a]	−1.64%[a]	−1.07%[a]	−1.73%[a]
15	0.58%[c]	1.11%[c]	0.69%[c]	0.73%[c]	0.71%[c]	0.84%[c]	−1.60%[a]	−1.82%[a]	−1.47%[a]	−1.78%[a]	−1.31%[a]	−1.84%[a]

[a]Values below −1%; [b]values between −1% and 0%; [c]values above 0%.

There is not a conclusive result on the link between batch repeatability with dimensional deviations. Although similar trends are shown in the final batches, this trend points towards homogeneity on measurements for all locations in both *x* and *y* directions. Therefore, powder reuse from this perspective does not seem to impact batch repeatability.

3.3. Part density

The density measurements following Archimedes' principle were conducted three times and the average density was divided by the theoretical density to obtain the cubes' relative density as plotted in the graph in Figure 6. The relative density values range from 99.6% to 100%. Batch 6, the last one to be built after a gas nozzle upgrade exhibits the lowest relative density values -on average-, but differences are very mild in most samples with a large spread in standard deviation. The upgrade effect is likely perceived better in lengthy and bulky builds in which gas flow plays a key role in avoiding condensates to contaminate the melt pool. The lowest value and largest variations are observed in sample 15, closest to the gas inlet. Overall, the density values are high for all density cubes reaching almost full density independently of the location of the sample and batch number.

3.4. Microstructure and porosity analysis

SEM image in backscattered electron mode showing the microstructure and porosity of samples 2 and 15 of batches 2, 4 and 6 are shown in Figure 7. As previous studies indicate [22] and [23], the microstructure of as-built Ti6Al4V depends on the cooling rate typically greater than 410 K s^{-1} for PBF-LB processes, which would result in martensite α′ formation as discussed by Agius et al. [24]. Oxygen and nitrogen are alpha stabilisers in Ti6Al4V parts and may increase the rate of martensitic transformation when reusing the powder in consecutive build cycles [25]. The microstructures of the samples from different batches are similar, while the porosity also agrees with the density measurements presented in Figure 5, in which the differences between the samples were minimal and the density was between 99.6 and 99.9%. Since sample 2 is located at the back left side of the build plate opposite to the gas inlet and sample 15 is located front right side of the build plate close to the gas inlet it is reasonable to assume a difference in gas flow velocity between them. The backside samples (2) would have suffered from low gas flow velocity and less cooling effect in comparison to the front side samples (15). Additionally, batch 6 which contains the samples built after the gas nozzle update exhibits minimal porosity in the images for samples 2 and 15, agreeing with Figure

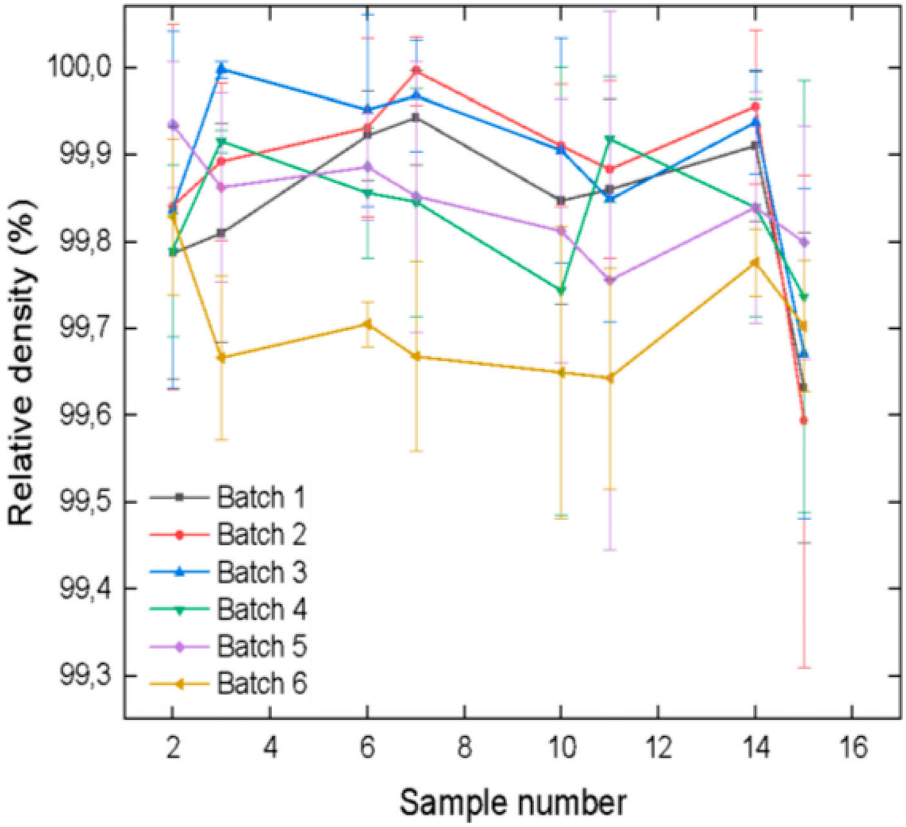

Figure 6. Density of consecutives builds measured by Archimedes principle.

5 in which the density values of all samples are compared.

4. Conclusions

In this study, the link between reusability and batch repeatability has been studied for Ti6Al4V ELI powder (grade 23) processed using a MetalFAB1 machine. The powder has been reused in the PBF-LB (powder bed fusion laser beam process) for at least 10 build cycles in which six of the build cycles were used to build cubes to track dimensional deviations and density throughout selected locations on the build plate. In general, the reusability of the powder has not been compromised, very mild variations were measured in particle size, morphology, and flowability and density. Hence, batch repeatability did not show large differences since the process parameters were the same and powder properties were very similar in an inert gas atmosphere. A summary of the main findings is listed below:

- Particle morphology and microstructural features in the cross-sections do not show large variations in the reused powder compared to the virgin one. The only difference was slight fewer fines spotted in the reused micrographs.
- Reuse powder shows a tendency to increase the particle size d50 and d90, which is considered a common effect of reuse.
- Bulk chemical composition of the main elements stays within the accepted range, from interstitial composition only oxygen content shows a tendency to increase.
- The flowability of the reused powder is slightly better, but the packing density shows similar values as well as the overall powder quality which has not been affected by reuse.
- Batch repeatability is shown by minor variations in dimensional deviation in consecutive batches. The observed deviations are – in general – negative in comparison with the nominal dimensions of the cubes. The first three batches built show a larger variability and the last three.
- The measured dimensions in the x and y direction of sample number 15, the closest to the gas nozzle show deviations in the positive direction unlike the rest of the samples.
- Building the cubes with two laser beams did not show relevant differences, either in the dimensional deviations nor in density values which remain similar to all batches and locations with large variations within high relative density between 99.96% and 100%.

In conclusion, powder reuse impact is minimised by the amount of powder that was initially loaded on the machine in combination with the high-purity inert gas used both for process and transport gas (PG, TG). This can also be seen on the high

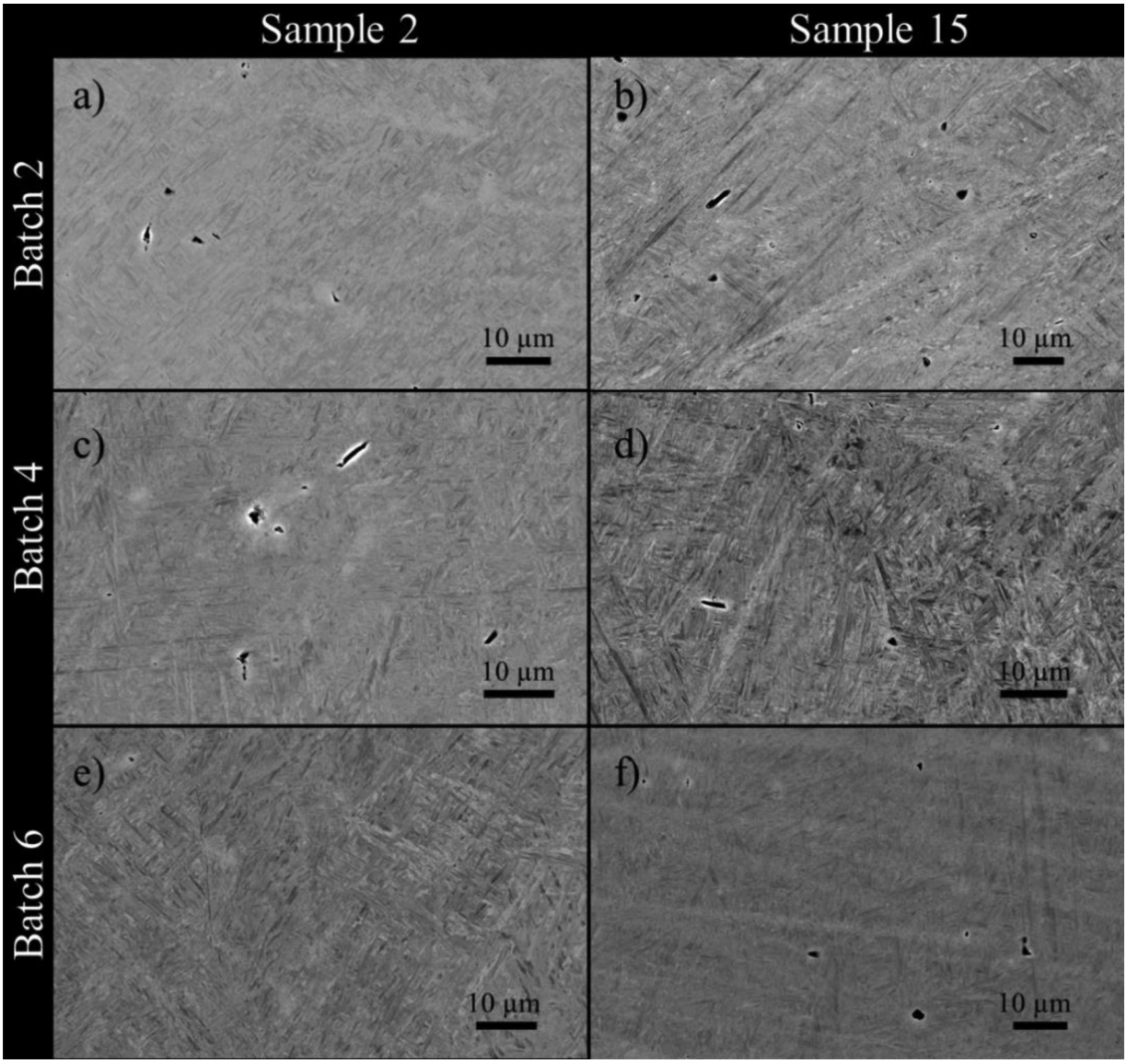

Figure 7. Microstructure and porosity of sample 2 (a, c, e) and sample 15 (b, d, f) built in batches 2, 4 and 6, respectively.

repeatability of dimensional accuracy and density within the build job and batch-to-batch. Since the jobs that have been performed were medium-to-low length and low in build efficiency, it is then recommended to test this powder at least every 10 cycles. A batch repeatability test with more complex parts placed on the corners or more sensitive areas of the build plate would allow more detail in future work. Due to the large size of the build plate, powder segregation can take place and gas flow dynamics vary, which could bring inhomogeneities to designs containing thin walls and overhangs.

Acknowledgements

This research has been supported by the Dutch Research Council (NWO) with the TKI – Connecting industry program under the project 'Development of flexible and integrated additive manufacturing systems'. The authors are grateful to Sandra Poelsma from Additive Industries for her support with machine operation.

Disclosure statement

No potential conflict of interest was reported by the author (s).

Funding

This work was supported by National Research Foundation of South Africa [grant number 120210]; Nederlandse Organisatie Voor Wetenschappelijk Onderzoek.

ORCID

Laura Cordova http://orcid.org/0000-0001-6982-4516
Ian Gibson http://orcid.org/0000-0002-4149-9122
Mónica Campos http://orcid.org/0000-0002-8360-9561

References

[1] Gibson I, Rosen DW, Stucker B. Additive manufacturing technologies. New York (NY): Springer; 2010.

[2] Ardila LC, Garciandia F, González-Díaz JB, et al. Effect of IN718 recycled powder reuse on properties of parts manufactured by means of selective laser melting. Phys Procedia. 2014;56:99–107. doi:10.1016/j.phpro.2014.08.152.
[3] Gasper AND, Hickman D, Ashcroft I, et al. Oxide and spatter powder formation during laser powder bed fusion of Hastelloy X. Powder Technol. 2019;354:333–337. doi:10.1016/J.POWTEC.2019.06.004.
[4] Gasper AND, et al. Spatter and oxide formation in laser powder bed fusion of Inconel 718. Addit Manuf. 2018;24:446–456. doi:10.1016/J.ADDMA.2018.09.032.
[5] Cordova L, Campos M, Tinga T. Revealing the effects of powder reuse for selective laser melting by powder characterization. JOM. 2019;71(3):1062–1072. doi:10.1007/s11837-018-3305-2.
[6] Mellin P, Shvab R, Strondl A, et al. COPGLOW and XPS investigation of recycled metal powder for selective laser melting. Powder Metall. 2017;60(3):223–231. doi:10.1080/00325899.2017.1296607.
[7] Sutton AT, Kriewall CS, Leu MC, et al. Powder characterisation techniques and effects of powder characteristics on part properties in powder-bed fusion processes. Virtual Phys Prototyp. 2017;12(1):3–29. doi:10.1080/17452759.2016.1250605.
[8] Cordova L, Bor T, de Smit M, et al. Effects of powder reuse on the microstructure and mechanical behaviour of Al–Mg–Sc–Zr alloy processed by laser powder bed fusion (LPBF). Addit Manuf. 2020;36, doi:10.1016/j.addma.2020.101625.
[9] Seyda V, Kaufmann N, Emmelmann C. Investigation of aging processes of Ti-6Al-4 V powder material in laser melting. Phys Procedia. 2012;39:425–431. doi:10.1016/j.phpro.2012.10.057.
[10] Tang HP, Qian M, Liu N, et al. Effect of powder reuse times on additive manufacturing of Ti-6Al-4V by selective electron beam melting. JOM. 2015;67(3):555–563. doi:10.1007/s11837-015-1300-4.
[11] O'Leary R, Setchi R, Prickett P, et al. An investigation into the recycling of Ti-6Al-4V powder used within SLM to improve sustainability. SDM2015 2nd Int Conf Sustain Des Manuf; 2015.
[12] Quintana OA, Alvarez J, Mcmillan R, et al. Effects of reusing Ti-6Al-4V powder in a selective laser melting additive system operated in an industrial setting. JOM. 2018;70(9):1863–1869. doi:10.1007/s11837-018-3011-0.
[13] Moghimian P, et al. Metal powders in additive manufacturing: A review on reusability and recyclability of common titanium, nickel and aluminum alloys. Addit Manuf. 2021;43:102017. doi:10.1016/j.addma.2021.102017.
[14] Denti L, Sola A, Defanti S, et al. Effect of powder recycling in laser-based powder bed fusion of Ti-6Al-4V. Manuf Technol. 2019;19(2):190–196. doi:10.21062/ujep/268.2019/a/1213-2489/mt/19/2/190.
[15] Harkin R, Wu H, Nikam S, et al. Powder reuse in laser-based powder Bed fusion of Ti6Al4V-changes in mechanical properties during a powder top-up regime. Materials (Basel). 2022;15(6):2238,: 10.3390/ma15062238.
[16] Alamos FJ, Schiltz J, Kozlovsky K, et al. Effect of powder reuse on mechanical properties of Ti-6Al-4V produced through selective laser melting. Int J Refract Met Hard Mater. 2020;91:105273, doi:10.1016/J.IJRMHM.2020.105273.
[17] Pauzon C, Dietrich K, Forêt P, et al. Control of residual oxygen of the process atmosphere during laser-powder bed fusion processing of Ti-6Al-4V. Addit Manuf. 2021;38:101765, doi:10.1016/J.ADDMA.2020.101765.
[18] Pauzon C, Raza A, Hryha E, et al. Oxygen balance during laser powder bed fusion of Alloy 718. Mater Des. 2021;201:109511, doi:10.1016/J.MATDES.2021.109511.
[19] Carr RL. Evaluating flow properties of solids. Chem Eng. 1965;72:163–168.
[20] Cordova L, Bor T, de Smit M, et al. Measuring the spreadability of pre-treated and moisturized powders for laser powder bed fusion. Addit Manuf. 2020;32:101082, doi:10.1016/J.ADDMA.2020.101082.
[21] Cordova L, Campos M, Tinga T. Assessment of moisture content and its influence on laser beam melting feedstock, 2017, [Online]. Available from: https://www.europm2017.com/.
[22] Shi X, Ma S, Liu C, et al. Selective laser melting-wire arc additive manufacturing hybrid fabrication of Ti-6Al-4V alloy: microstructure and mechanical properties. Mater Sci Eng A. 2017;684:196–204. doi:10.1016/J.MSEA.2016.12.065.
[23] Sun Y, Aindow M, Hebert RJ. Comparison of virgin Ti-6Al-4V powders for additive manufacturing. Addit Manuf. 2018;21:544–555. doi:10.1016/j.addma.2018.02.011.
[24] Agius D, Kourousis KI, Wallbrink C, et al. Cyclic plasticity and microstructure of as-built SLM Ti-6Al-4V: the effect of build orientation. Mater Sci Eng A. 2017;701:85–100. doi:10.1016/J.MSEA.2017.06.069.
[25] Harkin R, Wu H, Nikam S, et al. Reuse of grade 23 Ti6Al4V powder during the laser-based powder bed fusion process. Metals (Basel). 2020;10(12):1–14. doi:10.3390/met10121700.